LCLS-TN-00-14
October 3,2000

Electron Phase Slip in an Undulator with Dipole Field and BPM Errors

Paul Emma

SLAC

ABSTRACT

A statistical analysis of a corrected electron trajectory through a planar undulator is used to predict the optimal beam position monitor (BPM) spacing. The undulator is composed of multiple modular sections, each containing many dipoles with random field strength and roll angle errors. Located between each section are inaccurate BPMs, steering correctors, and quadrupole magnets. An analytical formula for electron-to-photon phase errors is derived and is also used to estimate the optimum BPM spacing. The rms trajectory amplitude is also predicted and the results are applied to the LCLS FEL undulator where the requirements on electron trajectory straightness are very demanding.

1 Introduction

The requirements on the degree of straightness of an electron trajectory through a SASE-based FEL undulator can be quite demanding. For short wavelength undulator radiation (1.5 Å in the LCLS [1]) a stringent requirement exists on the relative phase relationship between the electron beam and the radiated photon beam. Undulator field and beam position monitor (BPM) accuracy errors can force the electron beam to travel a longer path and thus phase-lag the photon beam. A significant phase error can move the electron beam away from resonance and negate the FEL gain. Since the location and number of BPMs along the undulator is an important factor in achieving a straight trajectory, it is useful to have a simple way in which to estimate the expected electron-to-photon phase errors and the rms trajectory amplitude, both as a function of BPM separation distance, BPM resolution, and dipole field errors. Previous work [2] has examined the effects of dipole errors, but the effects of inaccurate BPMs were not included.

We derive an analytical formula which can be used to estimate the optimal BPM separation along a planar undulator given the expected BPM resolution and dipole field errors. We also estimate the expected value of the rms electron trajectory anywhere along the undulator after steering using misaligned BPMs. Misaligned quadrupole magnets can also affect the trajectory, but steering corrections applied at, or very near, the quadrupoles can be used to completely compensate this component of the trajectory. Since the limit of this compensation is solely dependent on the resolution and transverse alignment of the BPMs, we can ignore quadrupole misalignments. They are implicitly included here in the steering corrections and the treatment of the BPM limitations. The effects of quadrupole magnets located in-between BPMs are, however, not covered here. Each quadrupole is assumed to have a nearby steering corrector and BPM in both planes.

The existence of an optimal spacing can be imagined by considering each type of error (BPM and dipole) in isolation. If the BPMs are inaccurate (misaligned or resolution limited), but the dipole fields are perfect, then a shorter BPM spacing forces a higher frequency trajectory distortion after steering correction (see left plot of Figure 1) [3]. The higher frequency implies larger trajectory angles between BPMs and therefore larger phase lag with respect to the radiated photon beam [see Eq. (10)]. In contrast, steering correction using perfect BPMs, but imperfect dipole fields, will generate a larger cumulative trajectory deviation between BPMs with a larger BPM spacing, again causing an increased phase lag (see right plot of Figure 1). BPM errors demand a long BPM spacing, while dipole errors suggest a short BPM spacing (for a constant undulator period). The goal here is to statistically estimate the optimum spacing, the expected trajectory amplitude, and the mean phase error.

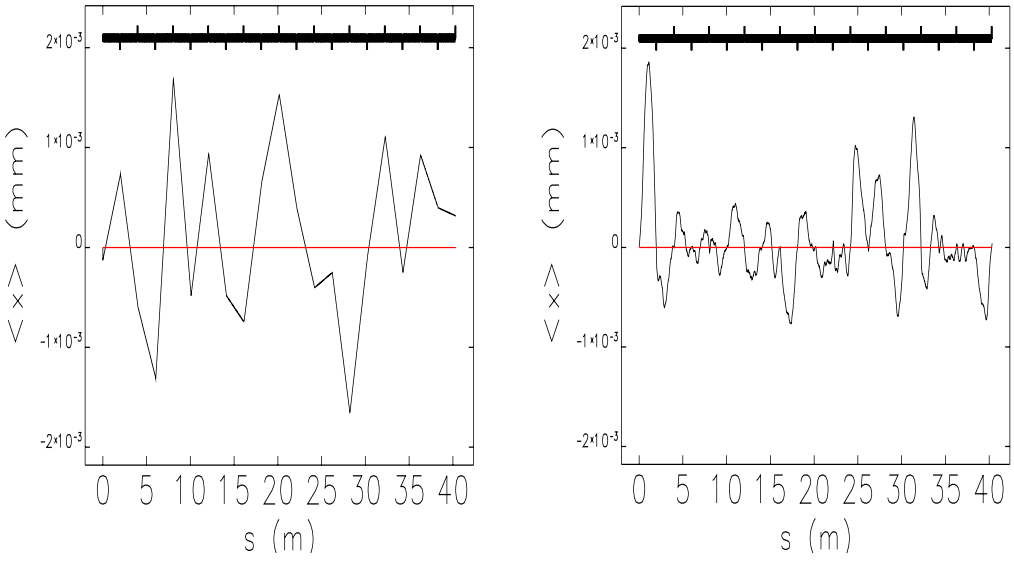

Figure 1. Steered undulator trajectory with BPM resolution of 1 μm rms, but perfect dipole fields (left), and steered trajectory with perfect BPM accuracy, but 0.1 % rms relative dipole field errors (right). A BPM, steering corrector, and quadrupole magnet are located approximately every 2 meters. Between BPMs there are 63 undulator periods of length 3 cm and field 1.3 T ($K \approx 3.7$) at 14.3 GeV.

2 Trajectory Analysis

A simplified planar undulator section is shown schematically below in Figure 2. The full undulator will be composed of multiple such sections.

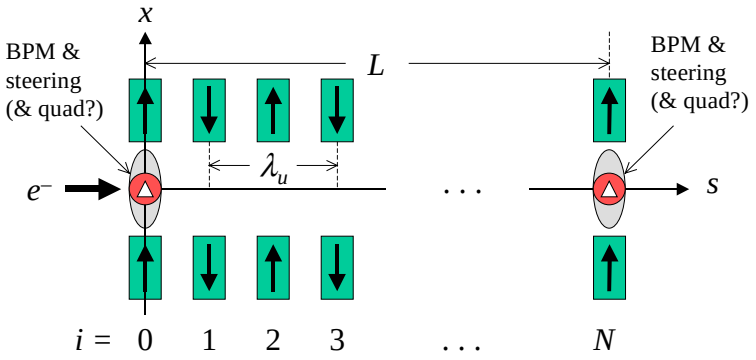

Figure 2. Simplified planar undulator section used to analyze the electron trajectory. The section has a length L with $N/2$ undulator periods and a BPM and steering corrector placed between each section. Quadrupole magnets may be located at or near the BPMs. Their effects are implicitly addressed here.

The section length is given by L, the undulator period is λ_u, and there are $N/2 = L/\lambda_u$ periods over the section (N dipoles). A BPM and a dipole steering element (or moveable quadrupole) are placed at each section boundary. For simplicity, this model includes no period breaks at the BPMs, and the details of wiggler termination at the start and end of a

section are ignored. Quadrupole magnets, if used, are assumed to be placed at or near the BPMs, but are not addressed here since their misalignments simply change the steering corrections required, and the focusing is not relevant for the single particle trajectory. The effect of an incoming betatron oscillation is also ignored since it can be removed at the undulator input with upstream steering or added later to these results as an independent effect. It is assumed that no significant focusing exists between the quadrupoles (*i.e.* within the undulator section), but such effects might be added in a future modified analysis.

A perfect undulator section (and a perfect initial trajectory) will produce a nominal *reference trajectory* which is composed of the small transverse oscillations normally associated with an undulator. This reference trajectory is subtracted off and only the difference trajectory produced by small dipole field errors and inaccurate steering is examined. Examples of such *difference* trajectories are shown in Figure 1 [4].

For a sinusoidal varying field with peak B_0 and relative field errors ($\Delta B_j/B_0$), each dipole error produces an additional e^- transverse kick at the center of the j^{th} dipole of

$$\theta_j = \frac{B_0 \lambda_u}{\pi (B\rho)} \left(\Delta B_j / B_0 \right) = \frac{2K}{\gamma} \left(\Delta B_j / B_0 \right), \tag{1}$$

where ($B\rho$) is the standard magnetic rigidity, γ is the Lorentz energy factor, K is the dimensionless undulator parameter ($K \approx 3.7$ for the LCLS),

$$K \equiv \frac{eB_0 \lambda_u}{2\pi mc}, \tag{2}$$

m is the electron rest mass, c is the speed of light, and e is the electron charge. Ignoring any weak focusing of the undulator fields (as in ref. [2]), each upstream kick at location j ($0 \le j < N$) displaces the electron beam at a downstream location i ($j < i \le N$) by $\Delta x_{ij} = \theta_j (s_i - s_j) = \lambda_u \theta_j (i - j)/2$. The sum over all upstream displacements, Δx_{ij}; plus the displacement, $\theta_c \lambda_u i/2$, produced by an initial beam angle, θ_c, at $j = 0$; plus an initial BPM-limited position, b_1, produces a trajectory position at location i of

$$x_i = \frac{\lambda_u}{2} \left[\theta_c i + \sum_{j=0}^{i} \theta_j (i - j) \right] + b_1 \ . \tag{3}$$

The angle θ_c (at $j = 0$) is the sum of (1) an incoming angle from the previous section, plus (2) a correction angle used to steer the trajectory to the next BPM (at section's end). The offset b_1 is the initial e^- beam position at $j = 0$ resulting from upstream steering of the trajectory to the first BPM offset, b_1. The BPM offset, b_1, can be interpreted as a transverse alignment error of the BPM, a noise component of the BPM reading, or both combined.

The angle, θ_c, is now defined by steering the trajectory so that the next BPM 'reads' zero. Since this next BPM has a different random offset, b_2, than the first BPM, the steering correction will produce $x_N = b_2$. Using Eq. (3) with $i = N$ and $x_N = b_2$, and solving for the angle produces

$$\theta_c = \frac{1}{N}\left\{\frac{2}{\lambda_u}(b_2 - b_1) - \sum_{j=0}^{N}\theta_j(N-j)\right\}. \tag{4}$$

Eq. (4) is now substituted into (3) and the steered trajectory at any location, i, is given by

$$x_i = \frac{\lambda_u}{2}\left[\frac{2i}{N\lambda_u}(b_2 - b_1) - \frac{i}{N}\sum_{j=0}^{N}\theta_j(N-j) + \sum_{j=0}^{i}\theta_j(i-j)\right] + b_1. \tag{5}$$

After some rearrangement Eq. (5) can be put into a form where one sum extends from $j = 0$ to $i - 1$, and a second sum extends from $j = i$ to N.

$$x_i = \frac{\lambda_u}{2N}\left[(i-N)\sum_{j=0}^{i-1} j\theta_j \;\; - i\sum_{j=i}^{N}\theta_j(N-j)\right] + \left(1 - \frac{i}{N}\right)b_1 + \frac{i}{N}b_2. \tag{6}$$

This represents the beam position at the i^{th} dipole and can now be used to calculate the trajectory and the electron-to-photon phase slip over an ensemble of undulator sections with random errors. We start the analysis with the phase slip considerations.

3 Trajectory Induced Phase Slip Errors

The path length difference of an electron with speed $v \approx c$ and angle x', with respect to a photon with zero angle, over a length l, is given, for small angles, by

$$\Delta s = l\sqrt{1 + x'^2} - l \approx \frac{x'^2 l}{2}. \tag{7}$$

The beam angle, x'_i, through the i^{th} pole-center to pole-center separation of length, $\lambda_u/2$, is

$$x'_i = \frac{2}{\lambda_u}(x_{i+1} - x_i). \tag{8}$$

Here we approximate the small kicks over a dipole field error as equivalent thin-kicks located at the dipole centers. This approximation will be justified in numerical comparisons to follow.

The positions x_i and x_{i+1} are taken from Eq. (6) and after some rearrangements, the beam angle x'_i can be written as

$$x_i' = \frac{1}{N}\left[\sum_{j=1}^{N} j\theta_j - N\sum_{j=i+1}^{N}\theta_j + \frac{2}{\lambda_u}(b_2 - b_1)\right]. \tag{9}$$

We now write the electron-to-photon 'phase' error at location i as $\Delta\varphi_i = 2\pi\Delta s_i/\lambda_r = k_r\Delta s_i$, where λ_r is the FEL radiation wavelength (1.5 Å for the LCLS) and k_r is the radiation wavenumber.

$$\Delta\varphi_i = k_r\lambda_u\frac{x_i'^2}{4} \tag{10}$$

The total phase error over the undulator section is just the sum of individual phase errors. Combining Eqs. (9) and (10), the total phase error, φ_s, over the undulator section, after steering using the inaccurate section-bounding BPMs, is

$$\varphi_s = \frac{k_r\lambda_u}{4N^2}\sum_{i=1}^{N}\left\{\sum_{j=1}^{N} j\theta_j - N\sum_{j=i+1}^{N}\theta_j + \frac{2}{\lambda_u}(b_2 - b_1)\right\}^2. \tag{11}$$

We now move toward a statistical analysis of the trajectory and therefore consider b_1, b_2, and the set of angles θ_j as random, uncorrelated variables (also with zero mean value).

$$\left\langle\theta_j^2\right\rangle = \left\langle\theta_k^2\right\rangle \equiv \left\langle\theta^2\right\rangle, \quad \left\langle b_1^2\right\rangle = \left\langle b_2^2\right\rangle \equiv \left\langle b^2\right\rangle, \quad \left\langle\theta_j\theta_k\right\rangle = \left\langle b_1 b_2\right\rangle = \left\langle\theta_j b_l\right\rangle = 0 \tag{12}$$

This is an important step. It implies that the rms BPM errors used here, $\langle b^2\rangle^{1/2}$, are the uncorrelated, random component of the relative misalignments of two BPMs separated by one undulator section. This includes static, relative, uncorrelated misalignments as well as BPM readback noise. It does not include, nor should it include, any relative misalignments on a scale longer than an undulator section or any correlated component of the misalignments. Realistic simulations of beam-based alignment (BBA) [5], [6] over the LCLS undulator indicate that the relative, uncorrelated, random misalignment of two adjacent BPMs can be reduced to very nearly the fundamental BPM noise level (*e.g.* 1 μm rms). We, therefore, do not need to evaluate the BPM alignment with respect to a straight line over the length of the entire undulator. We assume that BBA has been performed adequately, which is anyway a probable requirement for SASE saturation with such short wavelength FELs.

The total phase error in Eq. (11) is now manipulated using Eqs. (12) and the following relations for the sums of powers of integers.

$$\sum_{j=1}^{n} j = \frac{1}{2}n(n+1), \quad \sum_{j=1}^{n} j^2 = \frac{1}{6}n(n+1)(2n+1), \quad \sum_{j=1}^{n} j^3 = \frac{1}{4}n^2(n+1)^2 \tag{13}$$

The mean (averaged over many random undulator sections) total phase error, $\langle \varphi_s \rangle$, of one undulator section with $N/2$ periods ($N \geq 1$), random dipole errors, and resolution limited BPMs is given by

$$\langle \varphi_s \rangle = k_r \left[\frac{\lambda_u}{24} \left(N^2 + 5 \right) \left\langle \theta^2 \right\rangle + \frac{2}{N \lambda_u} \left\langle b^2 \right\rangle \right]. \tag{14}$$

This is the mean phase error per undulator section. The total mean phase error, $\langle \varphi \rangle$, over the entire undulator length, L_u (= $N_s L$), which is composed of N_s sections, is $\langle \varphi \rangle = \langle \varphi_s \rangle L_u / L$.

$$\langle \varphi \rangle \approx k_r L_u \left[\frac{L}{6 \lambda_u} \left\langle \theta^2 \right\rangle + \frac{1}{L^2} \left\langle b^2 \right\rangle \right] \tag{15}$$

Here we have scaled Eq. (14) by L_u/L, introduced the undulator section length $L = N\lambda_u/2$, and assumed $N^2 >> 5$. So far, this result includes trajectory errors in the wiggle-plane only (which we assume to be the horizontal plane).

Equation (15) shows the tradeoffs anticipated in the choice of an optimum section length, L. The section length appears in the numerator of the dipole error term (*i.e.* the $\langle \theta^2 \rangle$ term), but in the denominator of the BPM resolution term (*i.e.* the $\langle b^2 \rangle$ term). Therefore, as described in the introduction, a shorter section length increases the phase lag induced by BPM errors, but decreases the phase lag induced by dipole errors (for a constant period). The behavior of Eq. (15), per meter of undulator, is shown in Figure 3 for a BPM resolution of $\langle b^2 \rangle^{1/2} = 1\ \mu$m, and for relative dipole errors of $(\Delta B/B_0)_{\rm rms} = 0.1$ %, 0.05 %, and 0.025 %. Here the undulator period is 3 cm, the radiation wavelength is 1.5 Å, the undulator parameter is $K = 3.7$, and the energy is 14.3 GeV. The optimum BPM spacing, L, moves from 1.8 m at $(\Delta B/B_0)_{\rm rms} = 0.10$ %, to 4.4 m at $(\Delta B/B_0)_{\rm rms} = 0.025$ %. The data points shown with error bars are a Monte Carlo computer calculation [3] at $(\Delta B/B_0)_{\rm rms} = 0.10$ % over 1000 undulator sections, which is used for numerical confirmation of Eq. (15). Note, the rms kick angles, $\langle \theta^2 \rangle^{1/2}$, are related to the rms relative dipole field errors as

$$\left\langle \theta^2 \right\rangle^{1/2} = \frac{2K}{\gamma} \left\langle \left(\Delta B / B_0 \right)^2 \right\rangle^{1/2}. \tag{16}$$

The result of Eq. (15) can be differentiated with respect to L and set equal to zero in order to calculate the optimal BPM spacing, L_{opt}. In addition, we use Eq. (16) to make the result explicit in terms of the dipole field errors.

$$L_{opt} \approx \left(\frac{3 \lambda_u \gamma^2 \left\langle b^2 \right\rangle}{K^2 \left\langle \left(\Delta B / B_0 \right)^2 \right\rangle} \right)^{1/3} \tag{17}$$

For an expected level of random, uncorrelated dipole errors, and a given BPM resolution, the optimum BPM spacing can be predicted using Eq. (17).

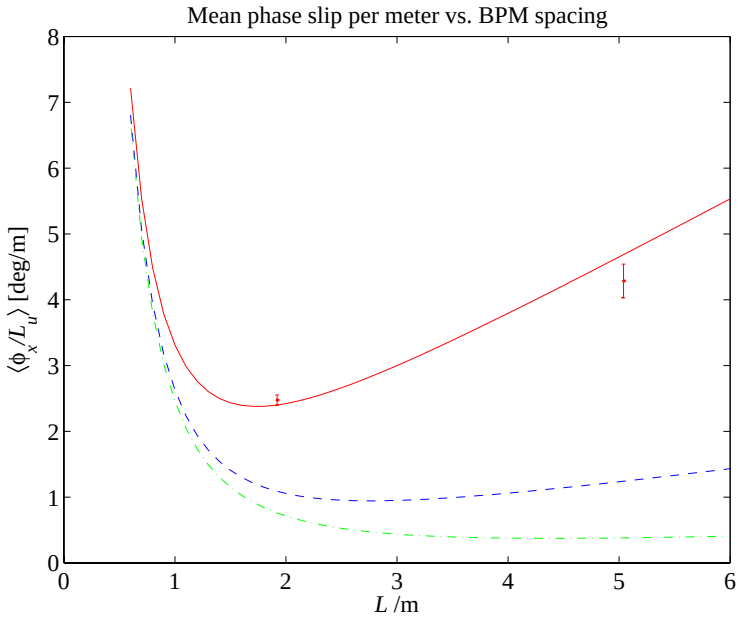

Figure 3. Mean phase error per meter of undulator [Eq. (15)] vs. undulator section length, L, for a BPM resolution of $\langle b^2\rangle^{1/2}$ = 1 μm, and dipole field errors of $(\Delta B/B_0)_{\rm rms}$ = 0.1 % (solid/red), 0.05 % (dash/blue), and 0.025 % (dash-dot/green). The optimum BPM spacing, L, moves from 1.8 m at 0.10 % to 4.4 m at 0.025 %. Points with error bars are a Monte Carlo computer calculation at 0.10 % used as a cross-check (λ_u = 3 cm, λ_r = 1.5 Å, K = 3.7, and γmc^2 = 14.3 GeV).

The argument can be extended into both horizontal and vertical planes by adding up the mean phase lag values per plane (*i.e.* $\langle\varphi_{xy}\rangle = \langle\varphi_x\rangle + \langle\varphi_y\rangle$). The additional mean phase lag due to vertical trajectory errors can be described by interpreting θ in Eq. (15) as a vertical kick, θ_y, due to a small random dipole roll-angle error, ψ, and the BPM term as the vertical resolution (equal to the horizontal resolution). The total mean phase lag over the length of the undulator, including horizontal and vertical trajectory errors, is then

$$\left\langle\varphi_{xy}\right\rangle \approx 2k_r L_u \left\{\frac{K^2 L}{3\gamma^2\lambda_u}\left[\left\langle\left(\Delta B/B_0\right)^2\right\rangle+\left\langle\psi^2\right\rangle\right]+\frac{1}{L^2}\left\langle b^2\right\rangle\right\}, \tag{18}$$

where the rms dipole roll angles, $\langle\psi^2\rangle^{1/2}$ (<< 1), are given by

$$\left\langle\theta_y^2\right\rangle^{1/2} = \frac{2K}{\gamma}\left\langle\psi^2\right\rangle^{1/2}. \tag{19}$$

Eq. (18) is simply twice that of Eq. (15) when $\langle(\Delta B/B_0)^2\rangle = \langle\psi^2\rangle$. In this case, the optimal spacing of Eq. (17) is still valid. If the rms field strength errors are significantly different from the rms roll angle errors, then Eq. (17) becomes

$$L_{opt} \approx \left(\frac{6\lambda_u \gamma^2 \left\langle b^2 \right\rangle}{K^2 \left[\left\langle \left(\Delta B / B_0 \right)^2 \right\rangle + \left\langle \psi^2 \right\rangle \right]} \right)^{1/3} . \tag{20}$$

From this point on we treat the case where $\langle \psi^2 \rangle = \langle (\Delta B/B_0)^2 \rangle$, for simplicity. Now substituting L_{opt} from Eq. (17) into L of Eq. (18) gives the minimum mean phase lag achieved at $L = L_{opt}$.

$$\left\langle \varphi_{xy} \right\rangle_{\min} = 2k_r L_u \left(\frac{3K^4 \left\langle b^2 \right\rangle \left\langle \left(\Delta B / B_0 \right)^2 \right\rangle^2}{\lambda_u^2 \gamma^4} \right)^{1/3} \tag{21}$$

The mean phase error should be kept below some tolerance level through quality control of both $\langle (\Delta B/B_0)^2 \rangle$ and $\langle b^2 \rangle$. Here we assume that a total phase error over the length of the undulator of $\langle \varphi_{xy} \rangle \leq 2\pi$ is a reasonable tolerance goal. This has been briefly studied for the LCLS parameters where it was found that a 2π net phase error increased the gain length by about 3 % [7]. This point needs further study, but we continue here with this simplifying assumption. In any case, the minimum phase lag is still achieved at the optimal BPM spacing described here.

If Eq. (21) is set to $\leq 2\pi$, the upper limit on the tolerable dipole field errors (and the roll angle errors) can be calculated, given the BPM resolution and radiation wavelength, λ_r, using

$$\left\langle \left(\Delta B / B_0 \right)^2 \right\rangle_{\text{tol}}^{1/2} \leq \frac{\gamma}{K} \sqrt{\frac{3\lambda_u}{8\left\langle b^2 \right\rangle^{1/2}}} \left(\frac{2\lambda_r}{3L_u} \right)^{3/4} . \tag{22}$$

This result can be re-substituted into Eq. (17) and the optimal BPM spacing can be calculated from knowledge only of the BPM resolution.

$$L_{opt} = \sqrt{\frac{6L_u}{\lambda_r}} \left\langle b^2 \right\rangle^{1/2} \tag{23}$$

In this case, the dipole field (and roll angle) tolerances are dependent variables prescribed by Eq. (22). The undulator design can therefore be initiated using just the knowledge of the expected BPM resolution.

As an example, Figure 4 shows the optimal BPM spacing [Eq. (23)] and the tolerable dipole field errors [Eq. (22)] as a function of BPM resolution. The optimal BPM spacing is linearly dependent on the BPM resolution, $\langle b^2 \rangle^{1/2}$. For this plot: L_u = 100 m, λ_r = 1.5 Å, λ_u = 3 cm, K = 3.7, and γmc^2 = 14.3 GeV. For example, a 4-μm BPM resolution requires

rms dipole field errors ≤0.04 % (and rms roll errors ≤0.4 mrad), and has an optimal BPM spacing of 8 m, while a 1-μm BPM resolution requires rms dipole field errors ≤0.08 % (and rms roll errors ≤0.8 mrad), and has an optimal BPM spacing of 2 m.

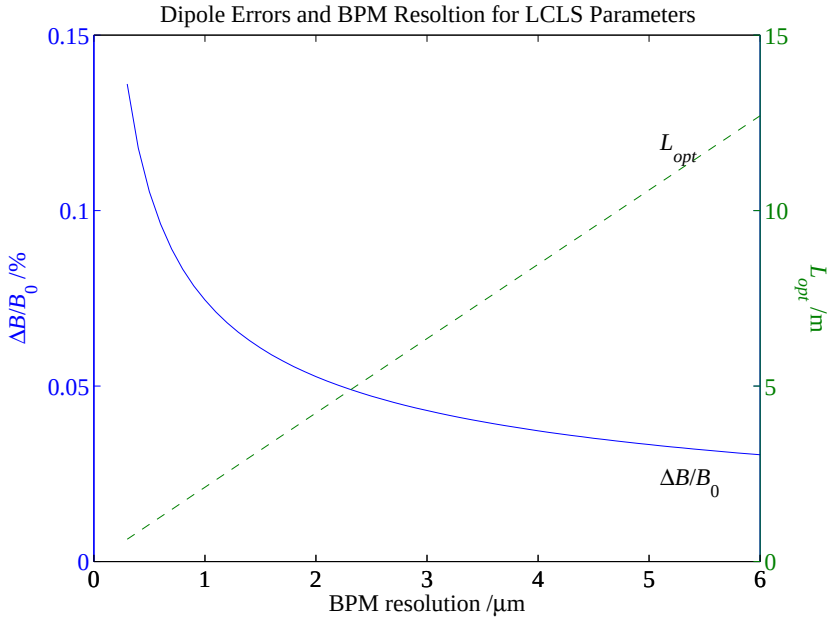

Figure 4. Tolerable dipole field errors (left scale; solid/blue) and optimal section length (right scale; dash/green) vs. BPM resolution for a net 2π mean phase lag over the undulator length (L_u = 100 m, λ_r = 1.5 Å, λ_u = 3 cm, K = 3.7, and γmc^2 = 14.3 GeV).

Likewise, if the dipole errors are known in advance, and the required BPM resolution is sought, then Eq. (21) can be rearranged as

$$\left\langle b^2 \right\rangle_{\text{tol}}^{1/2} \le \frac{3\gamma^2 \lambda_u}{8K^2 \left\langle \left(\Delta B/B_0\right)^2 \right\rangle} \left(\frac{2\lambda_r}{3L_u} \right)^{3/2}, \tag{24}$$

where the tolerance of $\langle \varphi_{xy} \rangle \le 2\pi$ is still assumed. From this, the optimal BPM spacing can be taken directly from the dipole errors, rather than from the BPM resolution as in Eq. (23).

$$L_{opt} = \frac{\lambda_r \lambda_u \gamma^2}{2K^2 L_u \left\langle \left(\Delta B/B_0\right)^2 \right\rangle} \tag{25}$$

These results can be compared to the numerical study done by H.-D. Nuhn using FRED-3D which is published in the LCLS Design Study Report [1]. Here the optimal BPM spacing was found by applying 0.1 % random dipole errors and various BPM resolution limitations. At a BPM resolution of 1 μm, the optimal spacing was found around 2 m, which is in reasonable agreement with 1.7 m from Eq. (17).

The dipole errors, however, can typically be controlled to a much better level by magnetic measurements and shimming techniques [8], [9], [10]. Using such techniques can greatly reduce the uncorrelated random component of the dipole field errors, which are used here to calculate the optimal spacing, and as such will tend to argue for much larger BPM spacing. The focusing lattice must, however, also be taken into account when increasing the BPM/quadrupole spacing, since, for a FODO-lattice, this will also increase the mean beta function, or increase the ratio of β_{max}/β_{min}. A focusing lattice composed of quadrupole triplets can take advantage of the longer section lengths [11], but the internal alignment tolerances within the triplet assembly can be extremely tight [12].

4 Trajectory Amplitude

We can also analyze the amplitude of the electron trajectory, which may have some significance when considering the spatial overlap of the electron and photon beams. The beam position at the i^{th} dipole in Eq. (6) is now used to calculate the rms trajectory amplitude over an ensemble of undulator sections with random errors. The form in Eq. (6) is convenient since it is a linear combination of uncorrelated, random variables and its variance, $\langle x^2 \rangle$, is simply the sum in quadrature of the components. The variance, or the expectation value of the square of the electron trajectory over an ensemble of sections, is then written as

$$\left\langle x_i^2 \right\rangle = \frac{\lambda_u^2}{4N^2}\left\langle \theta^2 \right\rangle \left[(i-N)^2 \sum_{j=0}^{i-1} j^2 \; + i^2 \sum_{j=i}^{N} (N-j)^2 \right] + \frac{1}{N^2}\left\langle b^2 \right\rangle \left[(N-i)^2 + i^2 \right], \qquad (26)$$

where we have used Eq. (12) for the uncorrelated random variables.

Eq. (26) is reduced to a polynomial in i by applying the summation relations of Eq. (13). The rms kick angles are also replaced by the rms dipole errors given by Eq. (16).

$$\left\langle x_i^2 \right\rangle = \frac{\lambda_u^2 K^2}{6N\gamma^2}\left\langle \left(\frac{\Delta B}{B_0} \right)^2 \right\rangle i\left[2i^3 - 4Ni^2 + (2N^2 - 1)i + N \right] + \frac{1}{N^2}\left\langle b^2 \right\rangle \left[2i^2 - 2Ni + N^2 \right] \qquad (27)$$

The index, i, is replaced by the longitudinal axis, s (= $i\lambda_u/2$), along the undulator section, and the number of dipoles, N (= $2L/\lambda_u$), is replaced by the section length, L. With zero-mean errors, $\langle\theta\rangle = \langle b \rangle = 0$, the rms trajectory is: $x_{rms} = \langle x^2 \rangle^{1/2}$, and Eq. (27) becomes

$$x_{rms}^2(s) = \frac{L^3 K^2}{3\lambda_u \gamma^2}\left\langle \left(\frac{\Delta B}{B_0} \right)^2 \right\rangle (s/L)\left[8(s/L)^3 - 16(s/L)^2 + \left(8 - \frac{\lambda_u^2}{L^2} \right)(s/L) + \frac{\lambda_u^2}{L^2} \right] + \left\langle b^2 \right\rangle \left[2(s/L)^2 - 2(s/L) + 1 \right]. \qquad (28)$$

For an undulator section with many dipole periods (*i.e.* $\lambda_u << L$), the rms trajectory anywhere along a section ($0 \le s \le L$) then simplifies to

$$x_{rms}(s) \cong \sqrt{\left[\frac{8}{3}\frac{L^3K^2}{\lambda_u\gamma^2}\left\langle\left(\Delta B/B_0\right)^2\right\rangle(s/L)^2 + \left\langle b^2\right\rangle\right]\left\{1-s/L\right\}^2 + \left\langle b^2\right\rangle(s/L)^2} \quad . \tag{29}$$

The peak, mid-section value of the rms trajectory, $\hat{x}_{rms}$, is taken at $s/L = ½$.

$$\hat{x}_{rms} \cong \frac{1}{\sqrt{2}}\sqrt{\frac{L^3K^2}{3\lambda_u\gamma^2}\left\langle\left(\Delta B/B_0\right)^2\right\rangle + \left\langle b^2\right\rangle} \tag{30}$$

The rms trajectory in Eq. (29) is a function of *s* since the rms is taken over an ensemble of undulator sections rather than over *s*. We can also integrate out the *s*-dependence by calculating the rms of Eq. (29) over the entire section length. This produces a single global rms value for the entire undulator trajectory integrated over both *s* and over many random seeds. The global rms value is given by integrating the square of Eq. (29) over the section length.

$$\left\langle x_{rms}^2\right\rangle_s^{1/2} \equiv \sqrt{\frac{1}{L}\int_0^L x_{rms}^2 ds} \cong \frac{2}{3}\sqrt{\frac{L^3K^2}{5\lambda_u\gamma^2}\left\langle\left(\Delta B/B_0\right)^2\right\rangle + \frac{3}{2}\left\langle b^2\right\rangle} \quad . \tag{31}$$

Eq. (29) is compared with computer generated trajectories in Figure 5 using 1000 random seeds and for various values of $\langle b^2\rangle$. The simulations propagate the beam trajectory continuously through 1000 consecutive undulator sections, ignoring any weak field gradients, but otherwise using an accurate model. These are difference trajectories with respect to the reference particle and do not include the nominal trajectory wiggles. Equation (29) is shown as a dashed curve (red) in each plot, and the rms over 1000 computer generated steered sections is shown as a solid curve (blue). Since $\lambda_u/L \approx 0.02$ (<< 1), the results of Eq. (28) and (29) are virtually identical and agree well with the time consuming computer calculations. The computer calculated values of the global rms (rms over the entire simulated trajectory) are also listed at the top of each plot. These values each agree with Eq. (31) to within <2%.

Eq. (31) demonstrates the somewhat obvious fact that the trajectory can be dominated by large BPM misalignments after applying one-to-one steering. That is, for BPMs of poor resolution,

$$\left\langle b^2\right\rangle^{1/2} > \frac{K}{\gamma}\sqrt{\frac{2L^3}{15\lambda_u}}\left\langle\left(\Delta B/B_0\right)^2\right\rangle^{1/2}, \tag{32}$$

the trajectory amplitude is BPM-dominated and the relative dipole errors play a less important role. In this case, the rms of the trajectory simplifies to

$$\left\langle x_{rms}^2 \right\rangle_s^{1/2} \approx \sqrt{\frac{2}{3}} \left\langle b^2 \right\rangle^{1/2} . \tag{33}$$

For a 2-m BPM spacing, Eq. (32) evaluates to ~0.8 μm at λ_u = 3 cm, K = 3.7, and γmc^2 = 14.3 GeV, and 0.1 % rms relative dipole errors, which means that a 1-μm resolution BPM, even if it is perfectly aligned, will still dominate the trajectory errors.

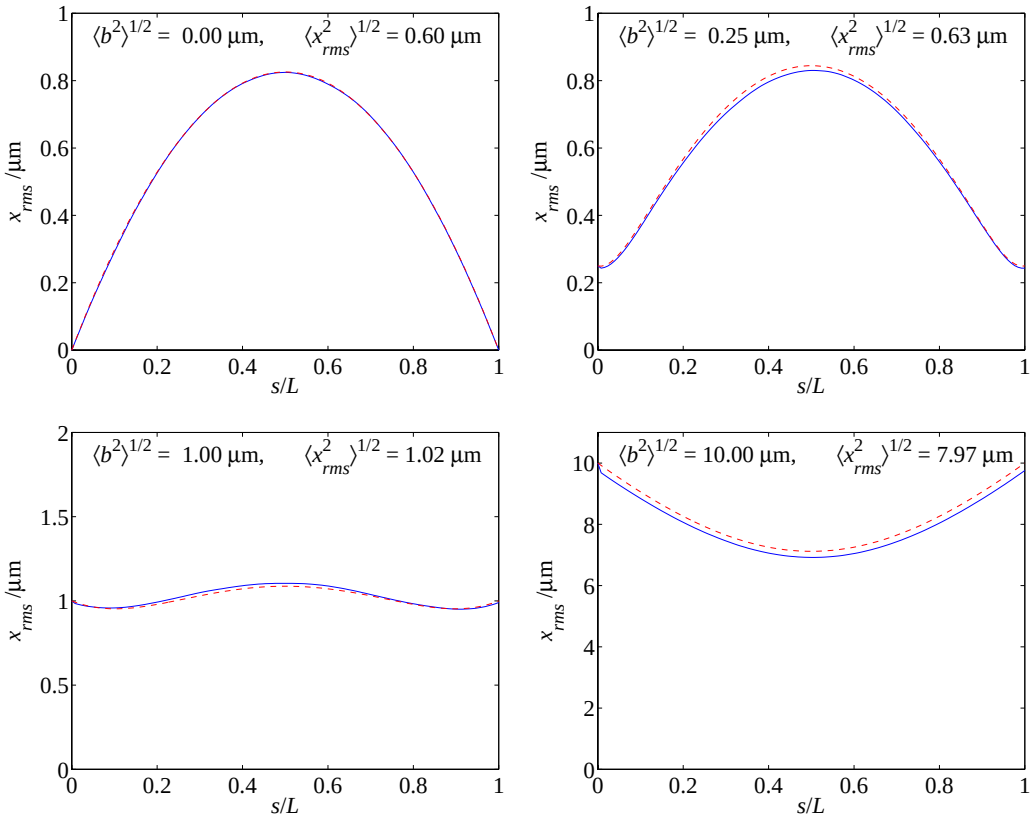

Figure 5. Trajectory rms over an undulator section showing the analytical result of Eq. (29) (dashed/red) and a computer calculation over 1000 random seeds (solid/blue). The four figures are for four different values of rms BPM errors, $\langle b^2 \rangle^{1/2}$ (= 0, 0.25, 1 and 10 μm), as shown on the plots, and λ_u = 3 cm, L = 1.92 m, K = 3.7, $\langle (\Delta B/B_0)^2 \rangle^{1/2}$ = 0.1%, and γmc^2 = 14.3 GeV.

It may also be interesting to ask which of the plots in Figure 5 best represent the minimal phase error conditions. Substituting L_{opt} from Eq. (23) into L in Eq. (30) and using Eq. (22) to describe the dipole errors, we find the peak rms-trajectory amplitude, at s/L = ½, is simply the BPM resolution

$$\hat{x}_{rms\,opt} \cong \left\langle b^2 \right\rangle^{1/2} , \tag{34}$$

and the global rms over the entire undulator, Eq. (31), is very nearly the BPM resolution.

$$\left\langle x_{rms}^2 \right\rangle_{s_{opt}}^{1/2} \cong \sqrt{\frac{14}{15}} \left\langle b^2 \right\rangle^{1/2} \tag{35}$$

This situation is depicted qualitatively (not precisely optimum) in the lower-left plot of Figure 5, which shows the almost intuitive result that minimal phase errors are achieved for the flattest trajectory rms. This situation is very similar to the criterion for beta function variations in the undulator where the best conditions require the smoothest beta functions.

It is worth noting that for typical LCLS parameters and tolerances, the predicted rms trajectory amplitude is 1-2 μm, yet the mean rms beam size is ~30 μm. The electron/photon beam spatial overlap then appears to be quite good, yet the potential phase errors are beginning to affect the gain. For very short wavelength radiation the spatial overlap may be of less concern than the phase slip.

Of course, knowledge of the rms trajectory amplitude and phase errors is not enough to fully evaluate the FEL performance. The beta function is also an important parameter which is related to the BPM/quadrupole spacing. For well controlled pole errors and conservative values of BPM resolution, these conclusions would tend to push the BPM spacing toward the longer limits set by mean beta function and $\beta_{\max}/\beta_{\min}$ considerations.

5 Conclusions

For an FEL undulator composed of separate sections which are bounded by BPMs, steering correctors, and quadrupole magnets, the undulator section length can be optimized analytically using Eq. (23) [or (25)], with knowledge of the undulator length, the radiation wavelength, and the expected BPM resolution [or dipole field and roll errors]. The dipole field and roll angle tolerances [or BPM resolution requirements] are then given by Eq. (22) [or (24)]. This assumes that beam-based alignment has been performed to align the BPMs, with respect to their nearest neighbors, to the level of their resolution. Well controlled pole errors, as might be produced using shimming methods, will increase the optimal section length by reducing the dipole field and roll errors. The mean beta function, and its variation, must, however, also be considered. A FODO-lattice for the LCLS ($L_u \approx 120$ m, $\lambda_u = 3$ cm, $\lambda_r = 1.5$ Å, $K = 3.7$, $\gamma mc^2 = 14.3$ GeV), with (for example) 0.05-% random uncorrelated pole field errors (and 0.5-mrad roll errors) has an optimal section length of 4.2 m (from the standpoint of trajectory errors alone), and a BPM resolution requirement of 2 μm. Such a system will, on average, produce a tolerable net 2π phase lag of the electron beam over the length of the undulator, with respect to the radiated x-ray beam, due to electron trajectory errors in both planes. A slightly shorter section length (*e.g.* 3-4 m) is, however, better suited to the requirements on the mean beta function.

6 Acknowledgements

I would like to thank Ilan Ben-Zvi and Max Cornacchia for encouraging this work, and Heinz-Dieter Nuhn for many helpful comments.

7 References

[1] *LCLS Design Study Report*, SLAC-R-521, April 1998.

[2] L.-H. Yu, et. al., *Effect of Wiggler Errors on Free-Electron-Laser Gain*, Physical Review A, Vol. 45, No. 2, January 15, 1992.

[3] These particle tracking calculations were performed using the computer code *Elegant* written by Michael Borland at Argonne National Laboratory.

[4] By examining the difference trajectory we have ignored the fact that it is also possible to find an electron trajectory which is advanced in phase, rather than retarded, with respect to the reference trajectory. Such an unlikely trajectory will follow a straighter path than the wiggling reference trajectory. The mean phase, however, will always be retarded. This has been confirmed in computer tracking.

[5] P. Emma, R. Carr, H.-D. Nuhn, *Beam Based Alignment For The LCLS FEL Undulator*, Proceedings of the 1998 Free Electron Laser Conference, Newport News, Virginia, August 1998.

[6] P. Castro, *TTF FEL Beam-based Alignment by Dispersion Correction Using Micado Algorithm*, TESLA-FEL 97-04, August, 1997.

[7] H.-D. Nuhn, private communication, March 2000.

[8] I. Vasserman, *A Shimming Technique for Improvement of the Spectral Performance of APS Undulator A*, LS-253, January 9, 1996.

[9] C.M. Fortgang, R.W. Warren, *Measurement and Correction of Magnetic Fields in Pulsed Slotted-Tube Microwigglers*, NIM A 341, pp. 436-439, 1994.

[10] R.W. Warren, *Limitations on the Use of the Pulsed-Wire Field Measuring Technique*, NIM A 272, pp. 257-263, 1998.

[11] N. Vinokurov, private communication, April 2000.

[12] P. Emma, H.-D. Nuhn, *Quadrupole Magnet Error Sensitivities for FODO-Cell and Triplet Lattices in the LCLS Undulator*, LCLS-TN-00-5, February 2000.